

Electronic Supporting Information

Catalytic Catechol Oxidation by Copper Complexes: Development of a Structure-Activity Relationship

Erica C.M. Ording-Wenker,^a Maxime A. Siegler,^b Martin Lutz,^c and Elisabeth Bouwman^{*a}

^a Leiden Institute of Chemistry, Gorlaeus Laboratories, Leiden University, P.O. Box 9502, 2300 RA Leiden, The Netherlands, e-mail: bouwman@chem.leidenuniv.nl

^b Department of Chemistry, Johns Hopkins University, Baltimore, Maryland 21218, United States

^c Bijvoet Centre for Biomolecular Research, Utrecht University, Padualaan 8, 3584 CH Utrecht, The Netherlands

* To whom correspondence should be addressed. E-mail: bouwman@chem.leidenuniv.nl

Table of Contents

S1. Experimental Section

Complex Synthesis of $[\text{Cu}^{\text{II}}(\text{L}^1\text{*SCH}_3)(\text{Cl})]_2(\text{CuCl}_4)$	p. S2
X-ray Structure Determination	p. S2
Figure S1. Synthesis scheme for L^1SL^1	p. S3
Figure S2. Synthesis scheme for $\text{L}^1\text{*SCH}_3$, L^2SCH_3 and L^3SCH_3	p. S3

S2. Crystallographic Data

Figure S3. Displacement ellipsoid plots of $[\text{Cu}^{\text{II}}_2(\text{L}^1\text{SSL}^1)(\text{Cl})_2]_n(\text{BF}_4)_{2n}$ and $[\text{Cu}^{\text{II}}_2(\text{L}^2\text{SSL}^2)(\text{Cl})_2]_n(\text{ClO}_4)_{2n}$	p. S4
Figure S4. Displacement ellipsoid plots of $[\text{Cu}^{\text{II}}(\text{L}^1\text{*SCH}_3)(\text{Cl})](\text{BF}_4)$ and $[\text{Cu}^{\text{II}}(\text{L}^1\text{*SCH}_3)(\text{Cl})]_2(\text{CuCl}_4)$	p. S5
Figure S5. Displacement ellipsoid plot of $[\text{Cu}^{\text{II}}(\text{L}^2\text{SCH}_3)(\text{Cl})](\text{BF}_4)$	p. S5
Figure S6. Displacement ellipsoid plot of $[\text{Cu}^{\text{II}}_2(\text{L}^1\text{C}_6\text{L}^1)(\text{Cl})_4]$	p. S5
Table S1. Crystallographic and structure refinement data for $[\text{Cu}^{\text{II}}_2(\text{L}^1\text{SSL}^1)(\text{Cl})_2]_n(\text{BF}_4)_{2n}$, $[\text{Cu}^{\text{II}}_2(\text{L}^2\text{SSL}^2)(\text{Cl})_2]_n(\text{ClO}_4)_{2n}$, $[\text{Cu}^{\text{II}}(\text{L}^1\text{*SCH}_3)(\text{Cl})](\text{BF}_4)$, $[\text{Cu}^{\text{II}}(\text{L}^1\text{*SCH}_3)(\text{Cl})]_2(\text{CuCl}_4)$ and $[\text{Cu}^{\text{II}}(\text{L}^2\text{SCH}_3)(\text{Cl})](\text{BF}_4)$.	p. S6
Table S2. Selected bond distances and angles for $[\text{Cu}^{\text{II}}_2(\text{L}^1\text{SSL}^1)(\text{Cl})_2]_n(\text{BF}_4)_{2n}$, $[\text{Cu}^{\text{II}}_2(\text{L}^2\text{SSL}^2)(\text{Cl})_2]_n(\text{ClO}_4)_{2n}$, $[\text{Cu}^{\text{II}}(\text{L}^1\text{*SCH}_3)(\text{Cl})](\text{BF}_4)$, $[\text{Cu}^{\text{II}}(\text{L}^1\text{*SCH}_3)(\text{Cl})]_2(\text{CuCl}_4)$ and $[\text{Cu}^{\text{II}}(\text{L}^2\text{SCH}_3)(\text{Cl})](\text{BF}_4)$	p. S7

S3. UV-vis

Figure S7. UV-vis spectra of synthesized Cu^{II} complexes	p. S8
Figure S8. UV-vis spectra of 3,5-DTBQ formation catalyzed by $[\text{Cu}^{\text{II}}_2(\text{L}^{\text{Pz}}\text{SSL}^{\text{Pz}})(\text{Cl})_2]_n(\text{BF}_4)_{2n}$	p. S9
Figure S9. UV-vis spectra of $[\text{Cu}^{\text{II}}_2(\text{L}^{\text{Pz}}\text{SSL}^{\text{Pz}})](\text{BF}_4)_4$ in the presence of different amounts of chlorides	p. S9
Figure S10. Absorption curves at 400 nm of 3,5-DTBQ formation catalyzed by $[\text{Cu}^{\text{II}}_2(\text{L}^{\text{Pz}}\text{SSL}^{\text{Pz}})](\text{BF}_4)_4$ in the presence of different amounts of chlorides	p. S9
Figure S11. Absorption curves at 400 nm of 3,5-DTBQ formation catalyzed by $[\text{Cu}^{\text{II}}_2(\text{L}^1\text{*SSL}^1\text{*})](\text{BF}_4)_4$ at different catalyst concentrations	p. S10

S4. Kinetics

Figure S12. Plot of substrate concentration vs. reaction rate for $[\text{Cu}^{\text{II}}(\text{L}^1\text{SCH}_3)](\text{BF}_4)$	p. S11
Figure S13. Plot of substrate concentration vs. reaction rate for $[\text{Cu}^{\text{II}}_2(\text{L}^1\text{*SSL}^1\text{*})](\text{BF}_4)_4$	p. S11

S1. Experimental section

*Synthesis of [Cu^{II}(L¹*SCH₃)(Cl)]₂(CuCl₄)*

L¹*SCH₃ (690 mg; 2.40 mmol) and Cu^{II}Cl₂ · 2 H₂O (614 mg; 3.60 mmol) were dissolved in 50 mL methanol and refluxed for 1 hour. The solution was cooled down and left to evaporate until green crystals had formed. The crystals were filtered and washed with methanol and diethyl ether to give [Cu^{II}(L¹*SCH₃)(Cl)]₂(CuCl₄) (789 mg; 0.807 mmol; 67%). Crystals suitable for X-ray structure determination were originally obtained from 1 instead of 1.5 equiv of Cu^{II}Cl₂ · 2 H₂O. ESI-MS found (calculated) for [½ M – CuCl₄]⁺ *m/z* 384.8 (385.0). IR (neat, cm⁻¹): 2932w, 1607s, 1573w, 1482m, 1440s, 1299m, 1284m, 1157m, 1053m, 1030s, 989w, 938w, 868m, 770s, 728w, 656w, 420s. Elemental analysis calcd for [Cu^{II}(L¹*SCH₃)(Cl)]₂(CuCl₄): C 39.29, H 4.33, N 8.59, S 6.56; Found: C 38.61, H 4.39, N 8.39, S 6.49. UV-vis in CH₃CN at 0.15 mM [Cu] concentration: 259 nm (ε = 12 100 M⁻¹ cm⁻¹), 305 nm (ε = 5 100 M⁻¹ cm⁻¹), 464 nm (ε = 750 M⁻¹ cm⁻¹), 700 nm (ε = 130 M⁻¹ cm⁻¹), 890 nm (ε = 190 M⁻¹ cm⁻¹).

X-ray Structure Determination

The reflection intensities for [Cu^{II}₂(L¹SSL¹)(Cl)₂]_n(BF₄)_{2n}, [Cu^{II}₂(L²SSL²)(Cl)₂]_n(ClO₄)_{2n} and [Cu^{II}(L¹*SCH₃)(Cl)]₂(CuCl₄) were measured using a KM4/Xcalibur (detector: Sapphire3) with enhanced graphite-monochromated Mo K α radiation (λ = 0.71073 Å) at 110(2) K under the program CrysAlisPro (Version 1.171.35.11 or 1.171.36.24 Agilent Technologies, 2011-2012). The same program was used to refine the cell dimensions and for data reduction. The structures were solved with the program SHELXS-97/SHELXS-2013 (Sheldrick, 2008/2013) and were refined on *F*² with SHELXL-97/SHELXL-2013 (Sheldrick, 2008/2013). Analytical numeric absorption corrections based on a multifaceted crystal model were applied using CrysAlisPro. The temperature of the data collection was controlled using the system Cryojet (manufactured by Oxford Instruments). The H atoms were placed at calculated positions using the instructions AFIX 13, AFIX 23, AFIX 43 or AFIX 137 with isotropic displacement parameters having 1.2 or 1.5 times *U*_{eq} of the attached C atoms. CCDC 1043172, 1043173 and 1043168 contain the supplementary crystallographic data for [Cu^{II}₂(L¹SSL¹)(Cl)₂]_n(BF₄)_{2n}, [Cu^{II}₂(L²SSL²)(Cl)₂]_n(ClO₄)_{2n} and [Cu^{II}(L¹*SCH₃)(Cl)]₂(CuCl₄). This data can be obtained free of charge from The Cambridge Crystallographic Data Centre via www.ccdc.cam.ac.uk/data_request/cif.

The reflection intensities for [Cu^{II}(L¹*SCH₃)(Cl)](BF₄) and [Cu^{II}(L²SCH₃)(Cl)](BF₄) were measured at 110(2) K using a SuperNova diffractometer (equipped with Atlas detector) with Cu K α radiation (λ = 1.54178 Å) under the program CrysAlisPro (Version 1.171.36.32 Agilent Technologies, 2013). The same program was used to refine the cell dimensions and for data reduction. The structures were solved with the program SHELXS-2013 (Sheldrick, 2013) and were refined on *F*² with SHELXL-2013 (Sheldrick, 2013). Analytical numeric absorption corrections based on a multifaceted crystal model were applied using CrysAlisPro. The temperature of the data collection was controlled using the system Cryojet (manufactured by Oxford Instruments). The H atoms were placed at calculated positions using the instructions AFIX 13, AFIX 23, AFIX 43 or AFIX 137 with isotropic displacement parameters having values 1.2 or 1.5 times *U*_{eq} of the attached C atoms. CCDC 1043167 and 1043169 contain the supplementary crystallographic data for [Cu^{II}(L¹*SCH₃)(Cl)](BF₄) and [Cu^{II}(L²SCH₃)(Cl)](BF₄).

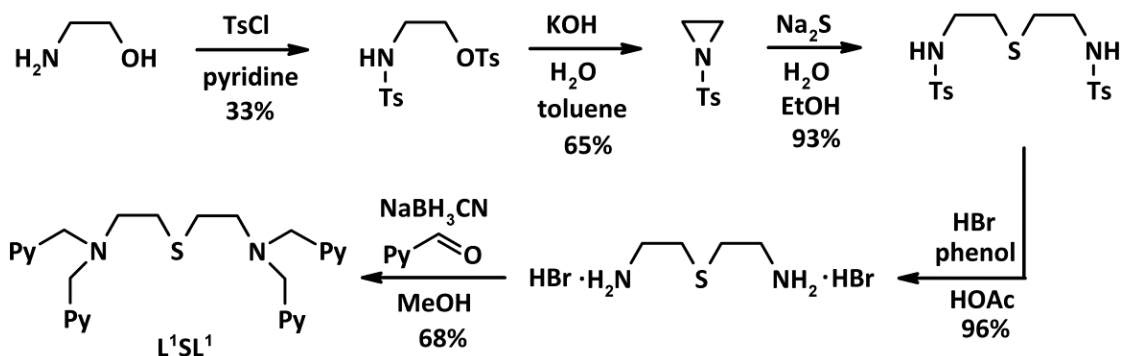


Figure S1. Synthesis scheme for L^1SL^1 (Herges et al., *Eur. J. Org. Chem.* **2002**, 3004-3014). Abbreviations: Ts = 4-toluenesulfonyl; Ac = acetyl; Py = 2-pyridyl.

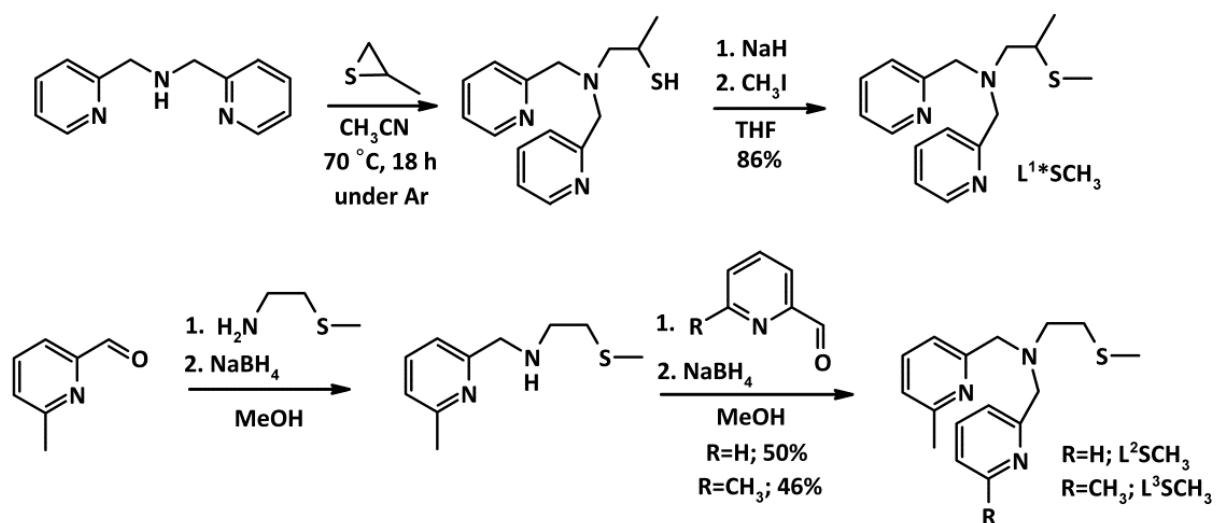


Figure S2. Synthesis scheme for L^1SCH_3 , L^2SCH_3 and L^3SCH_3 . Abbreviation THF = tetrahydrofuran.

S2. Crystallographic Data

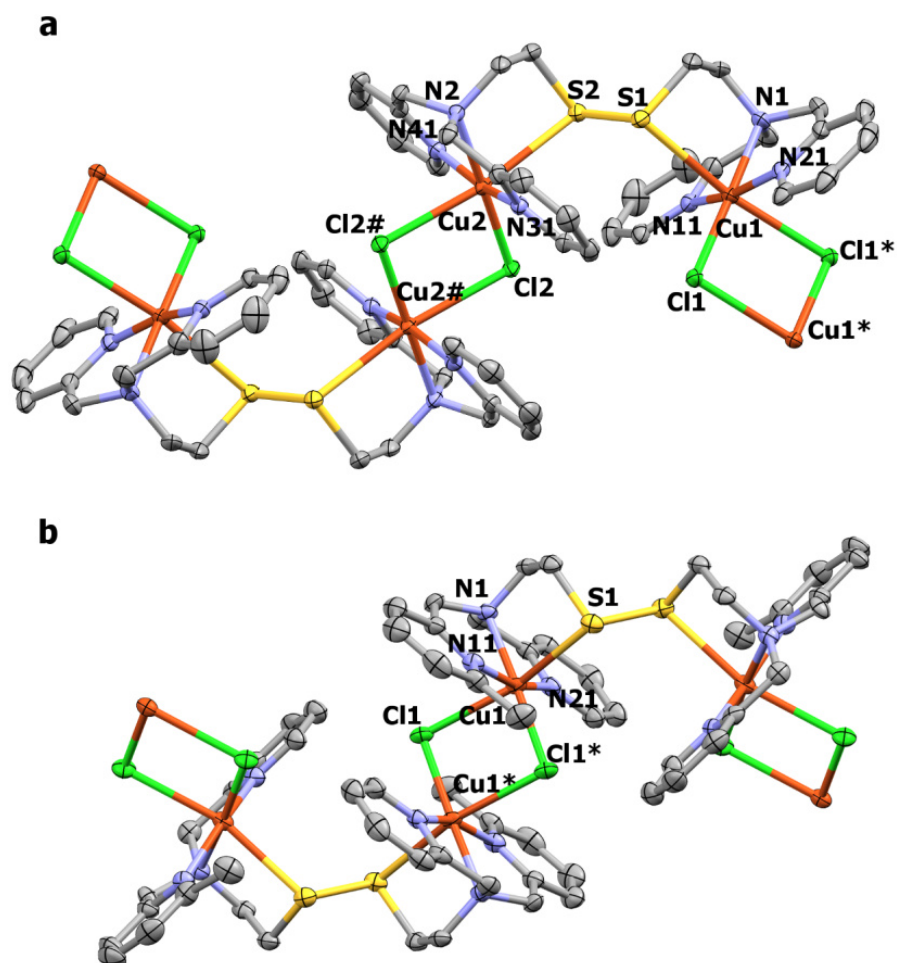


Figure S3. Displacement ellipsoid plots (50% probability level) of (a) $[\text{Cu}^{\text{II}}_2(\text{L}^1\text{SSL}^1)(\text{Cl})_2]_n(\text{BF}_4)_{2n}$ and (b) $[\text{Cu}^{\text{II}}_2(\text{L}^2\text{SSL}^2)(\text{Cl})_2]_n(\text{ClO}_4)_{2n}$ at 110(2) K. Hydrogen atoms, lattice solvent molecules (only for $[\text{Cu}^{\text{II}}_2(\text{L}^1\text{SSL}^1)(\text{Cl})_2]_n(\text{BF}_4)_{2n}$) and non-coordinating counterions are omitted for clarity. Symmetry operation * = $[-x, 1-y, 1-z]$ and # = $[-x, 1-y, -z]$ for $[\text{Cu}^{\text{II}}_2(\text{L}^1\text{SSL}^1)(\text{Cl})_2]_n(\text{BF}_4)_{2n}$. Symmetry operation * = $[1-x, 2-y, -z]$ for $[\text{Cu}^{\text{II}}_2(\text{L}^2\text{SSL}^2)(\text{Cl})_2]_n(\text{ClO}_4)_{2n}$.

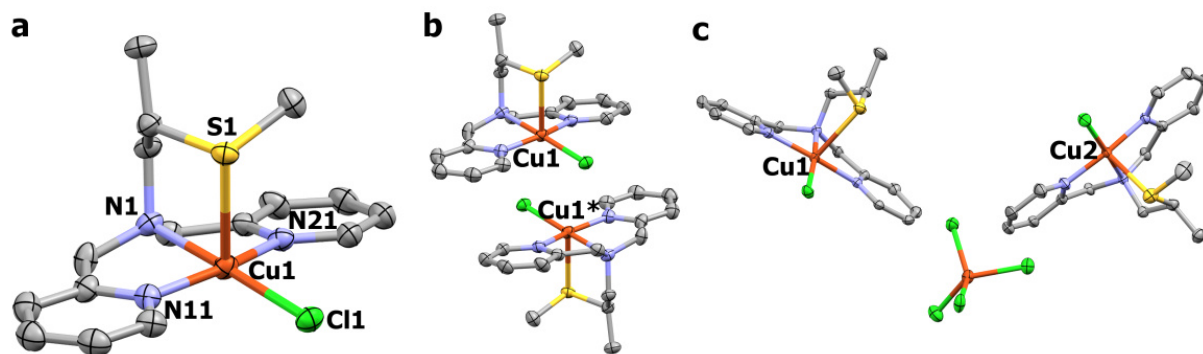


Figure S4. Displacement ellipsoid plots (50% probability level) of one (a) and two (b) cationic subunits of $[\text{Cu}^{\text{II}}(\text{L}^1*\text{SCH}_3)(\text{Cl})](\text{BF}_4)$ and of (c) $[\text{Cu}^{\text{II}}(\text{L}^1*\text{SCH}_3)(\text{Cl})]_2(\text{Cu}^{\text{II}}\text{Cl}_4)$ at 110(2) K. Disorder (only for $[\text{Cu}^{\text{II}}(\text{L}^1*\text{SCH}_3)(\text{Cl})](\text{BF}_4)$), hydrogen atoms and BF_4^- counterions have been omitted for clarity. Symmetry operation $*$ = $[2-x, -y, 1-z]$.

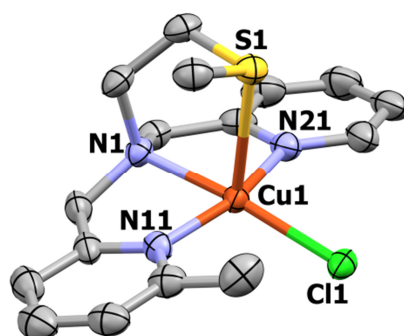


Figure S5. Displacement ellipsoid plot (50% probability level) of the cationic subunit of $[\text{Cu}^{\text{II}}(\text{L}^2\text{SCH}_3)(\text{Cl})](\text{BF}_4)$ at 110(2) K. Disorder, hydrogen atoms and non-coordinating counterions are omitted for clarity.

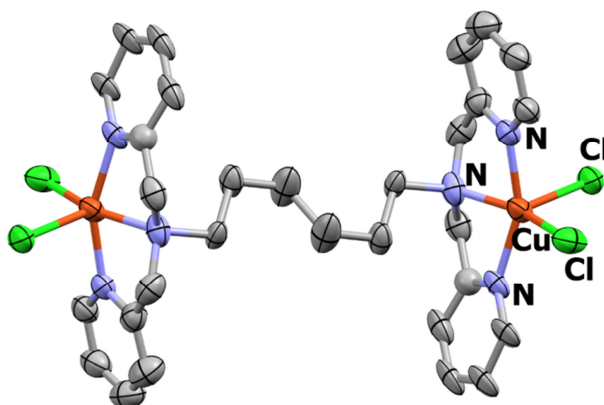


Figure S6. Displacement ellipsoid plot (50% probability level) of the reported complex $[\text{Cu}^{\text{II}}_2(\text{L}^1\text{C}_6\text{L}^1)(\text{Cl})_4]$ (E. C. M. Tse et.al., *Inorg. Chem.*, 2014, **53**, 8505-8516). Hydrogen atoms are omitted for clarity.

Table S1. Crystallographic and structure refinement data for complexes $[\text{Cu}^{\text{II}}_2(\text{L}^1\text{SSL}^1)(\text{Cl})_2]_n(\text{BF}_4)_{2n}$, $[\text{Cu}^{\text{II}}_2(\text{L}^2\text{SSL}^2)(\text{Cl})_2]_n(\text{ClO}_4)_{2n}$, $[\text{Cu}^{\text{II}}(\text{L}^1*\text{SCH}_3)(\text{Cl})](\text{BF}_4)$, $[\text{Cu}^{\text{II}}(\text{L}^1*\text{SCH}_3)(\text{Cl})]_2(\text{CuCl}_4)$ and $[\text{Cu}^{\text{II}}(\text{L}^2\text{SCH}_3)(\text{Cl})](\text{BF}_4)$.

	$[\text{Cu}^{\text{II}}_2(\text{L}^1\text{SSL}^1)(\text{Cl})_2]_n(\text{BF}_4)_{2n}$	$[\text{Cu}^{\text{II}}_2(\text{L}^2\text{SSL}^2)(\text{Cl})_2]_n(\text{ClO}_4)_{2n}$	$[\text{Cu}^{\text{II}}(\text{L}^1*\text{SCH}_3)(\text{Cl})](\text{BF}_4)$	$[\text{Cu}^{\text{II}}(\text{L}^1*\text{SCH}_3)(\text{Cl})]_2(\text{CuCl}_4)$	$[\text{Cu}^{\text{II}}(\text{L}^2\text{SCH}_3)(\text{Cl})](\text{BF}_4)$
empirical formula	$[\text{C}_{28}\text{H}_{32}\text{Cl}_2\text{Cu}_2\text{N}_6\text{S}_2](\text{BF}_4)_2 \cdot 2 \text{CH}_3\text{CN}$	$[\text{C}_{15}\text{H}_{18}\text{ClCuN}_3\text{S}](\text{ClO}_4)$	$[\text{C}_{16}\text{H}_{21}\text{ClCuN}_3\text{S}](\text{BF}_4)$	$[\text{C}_{16}\text{H}_{21}\text{ClCuN}_3\text{S}]_2(\text{CuCl}_4)$	$[\text{C}_{16}\text{H}_{21}\text{ClCuN}_3\text{S}](\text{BF}_4)$
formula weight	970.42	470.82	473.22	978.16	473.22
crystal system	triclinic	monoclinic	monoclinic	monoclinic	monoclinic
space group	<i>P</i> -1	<i>C</i> 2/ <i>c</i>	<i>P</i> 2 ₁ / <i>c</i>	<i>P</i> 2 ₁ / <i>n</i>	<i>C</i> 2/ <i>m</i>
<i>a</i> , Å	12.4006(2)	21.2487(5)	13.4189(4)	13.6254(3)	13.0671(3)
<i>b</i> , Å	13.1923(3)	12.6146(2)	12.5086(3)	13.2651(3)	20.2293(5)
<i>c</i> , Å	14.4294(4)	14.6206(4)	12.8357(5)	22.7359(5)	7.40187(15)
α , deg	104.022(2)	90	90	90	90
β , deg	107.238(2)	110.200(3)	116.644(4)	102.954(2)	101.660(2)
γ , deg	99.5150(18)	90	90	90	90
<i>V</i> , Å ³	2114.51(8)	3677.92(16)	1925.71(12)	4004.76(15)	1916.22(8)
<i>Z</i>	2	8	4	4	4
<i>D</i> _{calc} , g·cm ³	1.524	1.701	1.632	1.622	1.640
<i>T</i> , K	110(2)	110(2)	110(2)	110(2)	110(2)
crystal size, mm	0.57×0.42×0.26	0.19×0.19×0.17	0.17×0.12×0.02	0.52×0.35×0.15	0.35×0.28×0.20
μ , mm ⁻¹	1.301	1.618	4.297	2.116	4.318
no. of reflns measd	28931	13583	13585	27367	
no. of unique reflns	9699	3708	3754	8080	6657
no. of reflns obsd.	8706 [<i>I</i> > 2 σ (<i>I</i>)]	3303 [<i>I</i> > 2 σ (<i>I</i>)]	3206 [<i>I</i> > 2 σ (<i>I</i>)]	6596 [<i>I</i> > 2 σ (<i>I</i>)]	1913
no. of parameters	669	282	294	446	246
<i>R</i> ₁ / <i>wR</i> ₂ [<i>I</i> > 2 σ (<i>I</i>)]	0.0231/0.0620	0.0361/0.0930	0.0368/0.0889	0.0447/0.1218	0.0327/0.0861
<i>R</i> ₁ / <i>wR</i> ₂ [all refl.]	0.0266/0.0630	0.0413/0.0955	0.0455/0.0930	0.0573/0.1290	0.0346/0.0879
goodness of fit	1.074	1.058	1.041	1.051	1.046
$\Delta\rho$, e·Å ⁻³	-0.31/0.33	-0.39/0.87	-0.27/0.60	-1.08/2.62	-0.24/0.45

Table S2. Selected bond distances (Å) and bond angles (°) for complexes $[\text{Cu}^{\text{II}}_2(\text{L}^1\text{SSL}^1)(\text{Cl})_2]_n(\text{BF}_4)_{2n}$, $[\text{Cu}^{\text{II}}_2(\text{L}^2\text{SSL}^2)(\text{Cl})_2]_n(\text{ClO}_4)_{2n}$, $[\text{Cu}^{\text{II}}(\text{L}^1*\text{SCH}_3)(\text{Cl})](\text{BF}_4)$, $[\text{Cu}^{\text{II}}(\text{L}^1*\text{SCH}_3)(\text{Cl})]_2(\text{CuCl}_4)$ and $[\text{Cu}^{\text{II}}(\text{L}^2\text{SCH}_3)(\text{Cl})](\text{BF}_4)$.

	$[\text{Cu}^{\text{II}}_2(\text{L}^1\text{SSL}^1)(\text{Cl})_2]_n(\text{BF}_4)_{2n}$	$[\text{Cu}^{\text{II}}_2(\text{L}^2\text{SSL}^2)(\text{Cl})_2]_n(\text{ClO}_4)_{2n}$	$[\text{Cu}^{\text{II}}(\text{L}^1*\text{SCH}_3)(\text{Cl})](\text{BF}_4)$	$[\text{Cu}^{\text{II}}(\text{L}^1*\text{SCH}_3)(\text{Cl})]_2(\text{CuCl}_4)$	$[\text{Cu}^{\text{II}}(\text{L}^2\text{SCH}_3)(\text{Cl})](\text{BF}_4)$
Cu1 - Cu1*	3.5955(3)	3.6455(4)	3.7751(6)	3.9085(7)	3.8504(5)
Cu2 - Cu2#	3.6192(3)				
Cu1 - Cu2/Cu1#	5.6586(3)	5.6416(5)			
Cu1 - S1	2.8896(4)	2.7676(7)	2.645(3)	2.6608(11)	2.7260(9)
Cu1 - N1	2.0523(12)	2.041(2)	2.054(2)	2.054(3)	2.048(3)
Cu1 - N11	1.9803(12)	2.074(2)	2.003(2)	1.987(3)	2.046(5)
Cu1 - N21	1.9901(12)	2.028(2)	2.001(2)	1.985(3)	2.002(5)
Cu1 - Cl1	2.2666(4)	2.2644(7)	2.2662(7)	2.2594(10)	2.2586(8)
Cu1 - Cl1*	2.7862(4)	2.7428(8)	3.0985(8)	3.2663(12)	2.9837(9)
Cu2 - S2	2.8619(4)				
Cu2 - N2	2.0601(12)				
Cu2 - N31	1.9713(11)				
Cu2 - N41	1.9868(12)				
Cu2 - Cl2	2.2693(3)				
Cu2 - Cl2#	2.7719(3)				
S1 - Cu1 - N1	84.11(4)	85.43(7)	86.52(8)	85.49(9)	86.62(8)
S1 - Cu1 - N11	92.75(4)	77.40(7)	86.43(8)	102.36(10)	94.7(2)
S1 - Cu1 - N21	87.29(4)	100.67(7)	101.32(8)	86.22(9)	89.2(2)
S1 - Cu1 - Cl1/Cl1*	170.50(1)	164.24(2)	96.32(6)	101.22(4)	102.38(3)
N1 - Cu1 - N11	81.65(5)	82.10(9)	82.86(9)	81.61(13)	80.6(3)
N1 - Cu1 - N21	83.23(5)	81.20(9)	81.80(9)	84.00(13)	83.4(3)
N1 - Cu1 - Cl1	179.10(4)	174.37(7)	177.11(6)	173.26(9)	170.52(12)
N11 - Cu1 - N21	164.80(5)	163.29(9)	162.32(9)	162.57(14)	163.28(15)
S2 - Cu2 - N2	83.68(3)				
S2 - Cu2 - N31	93.92(4)				
S2 - Cu2 - N41	85.95(4)				
S2 - Cu2 - Cl2#	171.24(1)				
N2 - Cu2 - N31	82.10(5)				
N2 - Cu2 - N41	83.37(5)				
N2 - Cu2 - Cl2	179.11(4)				
N31 - Cu2 - N41	165.39(5)				

Symmetry operation * = $[-x, 1-y, 1-z]$ for $[\text{Cu}^{\text{II}}_2(\text{L}^1\text{SSL}^1)(\text{Cl})_2]_n(\text{BF}_4)_{2n}$; $[1-x, 2-y, -z]$ for $[\text{Cu}^{\text{II}}_2(\text{L}^2\text{SSL}^2)(\text{Cl})_2]_n(\text{ClO}_4)_{2n}$; $[2-x, -y, 1-z]$ for $[\text{Cu}^{\text{II}}(\text{L}^1*\text{SCH}_3)(\text{Cl})](\text{BF}_4)$; $[1-x, 1-y, -z]$ for $[\text{Cu}^{\text{II}}(\text{L}^1*\text{SCH}_3)(\text{Cl})]_2(\text{CuCl}_4)$; $[x, y, -1+z]$ for $[\text{Cu}^{\text{II}}(\text{L}^2\text{SCH}_3)(\text{Cl})](\text{BF}_4)$. Symmetry operation # = $[-x, 1-y, -z]$ for $[\text{Cu}^{\text{II}}_2(\text{L}^1\text{SSL}^1)(\text{Cl})_2]_n(\text{BF}_4)_{2n}$; $[1-x, y, \frac{1}{2}-z]$ for $[\text{Cu}^{\text{II}}_2(\text{L}^2\text{SSL}^2)(\text{Cl})_2]_n(\text{ClO}_4)_{2n}$.

S3. UV-vis

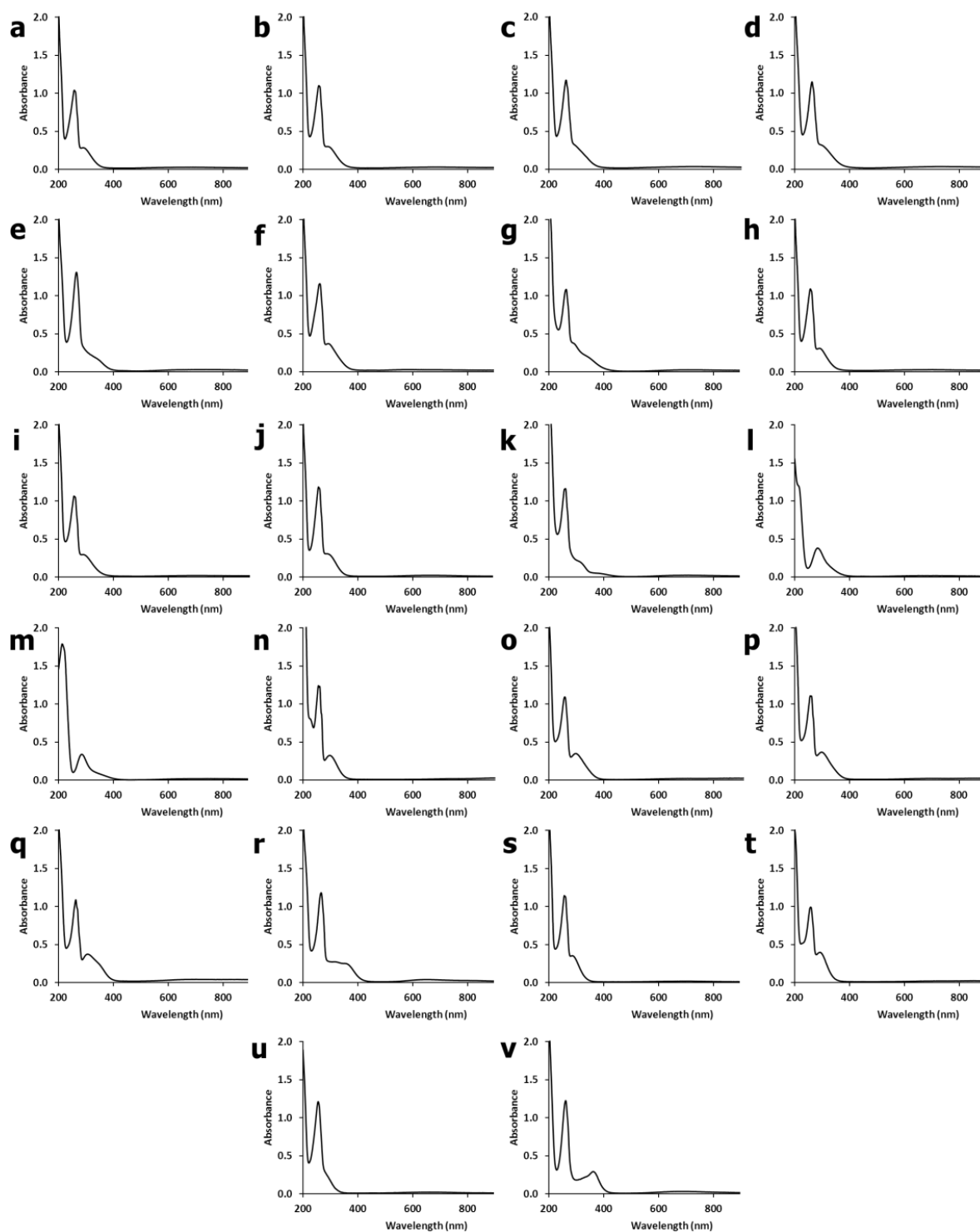


Figure S7. UV-vis spectra of (a) $[\text{Cu}^{\text{II}}_2(\text{L}^1\text{SSL}^1)(\text{Cl})_2]_n(\text{BF}_4)_{2n}$, (b) $[\text{Cu}^{\text{II}}_2(\text{L}^1*\text{SSL}^1*)(\text{Cl})_2]_n(\text{BF}_4)_{2n}$, (c) $[\text{Cu}^{\text{II}}_2(\text{L}^2\text{SSL}^2)(\text{Cl})_2]_n(\text{BF}_4)_{2n}$, (d) $[\text{Cu}^{\text{II}}_2(\text{L}^2*\text{SSL}^2*)(\text{Cl})_2]_n(\text{BF}_4)_{2n}$, (e) $[\text{Cu}^{\text{II}}_2(\text{L}^3\text{SSL}^3)(\text{Cl})_2]_n(\text{BF}_4)_{2n}$, (f) $[\text{Cu}^{\text{II}}_2(\text{L}^4\text{SSL}^4)(\text{Cl})_2]_n(\text{BF}_4)_{2n}$, (g) $[\text{Cu}^{\text{II}}_2(\text{L}^5\text{SSL}^5)(\text{Cl})_2]_n(\text{BF}_4)_{2n}$, (h) $[\text{Cu}^{\text{II}}_2(\text{L}^1\text{SXSL}^1)(\text{Cl})_2]_n(\text{BF}_4)_{2n}$, (i) $[\text{Cu}^{\text{II}}_2(\text{L}^1\text{SL}^1)(\text{Cl})_2]_n(\text{BF}_4)_{2n}$, (j) $[\text{Cu}^{\text{II}}_2(\text{L}^1\text{C}_6\text{L}^1)(\text{Cl})_2]_n(\text{BF}_4)_{2n}$, (k) $[\text{Cu}^{\text{II}}_2(\text{L}^1\text{PhL}^1)(\text{Cl})_2]_n(\text{BF}_4)_{2n}$, (l) $[\text{Cu}^{\text{II}}_2(\text{L}^{\text{Pz}}\text{SSL}^{\text{Pz}})(\text{Cl})_2]_n(\text{BF}_4)_{2n}$, (m) $[\text{Cu}^{\text{II}}_2(\text{L}^{\text{MPz}}\text{SSL}^{\text{MPz}})(\text{Cl})_2]_n(\text{BF}_4)_{2n}$, (n) $[\text{Cu}^{\text{II}}(\text{Py}_3\text{N})(\text{Cl})](\text{BF}_4)$, (o) $[\text{Cu}^{\text{II}}(\text{L}^1\text{SCH}_3)(\text{Cl})](\text{BF}_4)$, (p) $[\text{Cu}^{\text{II}}(\text{L}^1*\text{SCH}_3)(\text{Cl})](\text{BF}_4)$, (q) $[\text{Cu}^{\text{II}}(\text{L}^2\text{SCH}_3)(\text{Cl})](\text{BF}_4)$, (r) $[\text{Cu}^{\text{II}}(\text{L}^3\text{SCH}_3)(\text{Cl})](\text{BF}_4)$, (s) $[\text{Cu}^{\text{II}}(\text{L}^1\text{OH})(\text{Cl})](\text{BF}_4)$, (t) $[\text{Cu}^{\text{II}}(\text{L}^1\text{NH}_2)(\text{Cl})](\text{BF}_4)$, (u) $[\text{Cu}^{\text{II}}(\text{Py}_2\text{NH})(\text{Cl})](\text{BF}_4)$ and (v) $[\text{Cu}^{\text{II}}(\text{Py}_2\text{S})(\text{Cl})](\text{BF}_4)$ in CH_3CN at 0.1 mM $[\text{Cu}]$ concentration.

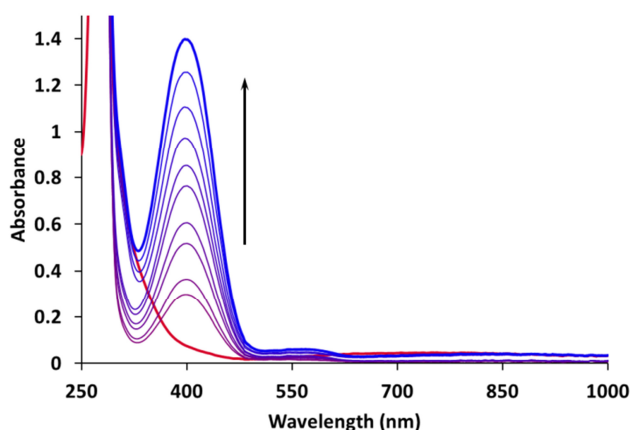


Figure S8. UV-vis spectra of 3,5-DTBQ formation catalyzed by $[\text{Cu}^{\text{II}}_2(\text{L}^{\text{PzSSL}}\text{Pz})(\text{Cl})_2]_n(\text{BF}_4)_{2n}$ at a concentration of 1.0 mM [Cu], 0.2 mM 3,5-DTBQ and 0.2 mM NEt_3 in CH_3CN over the course of 15 minutes. Spectra were recorded with a transmission dip probe path length of 2.0 mm.

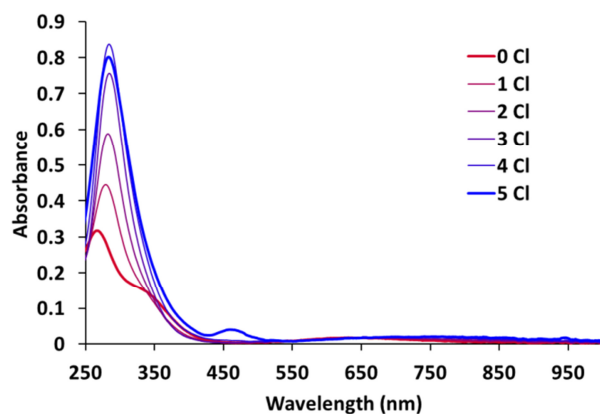


Figure S9. UV-vis spectra of $[\text{Cu}^{\text{II}}_2(\text{L}^{\text{PzSSL}}\text{Pz})](\text{BF}_4)_4$ in CH_3CN at 1.0 mM [Cu] concentration with 0 to 5 equiv of Bu_4NCl in ratio to the whole complex. Spectra were recorded with a transmission dip probe path length of 2.0 mm.

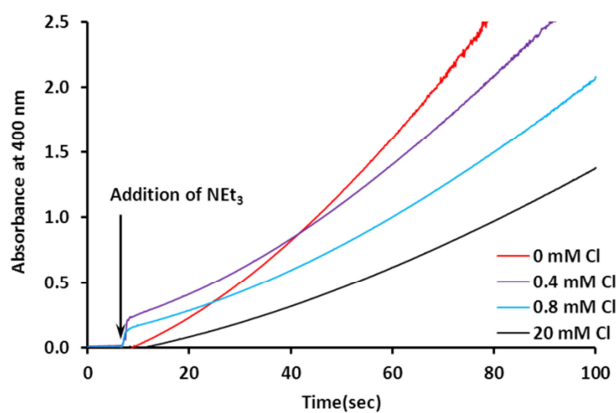


Figure S10. Absorption curves at 400 nm of 3,5-DTBQ formation, catalyzed by $[\text{Cu}^{\text{II}}_2(\text{L}^{\text{PzSSL}}\text{Pz})](\text{BF}_4)_4$ in the presence of 0 mM Cl^- (red), 0.4 mM Cl^- (purple), 0.8 mM Cl^- (blue) and 20 mM Cl^- (black).

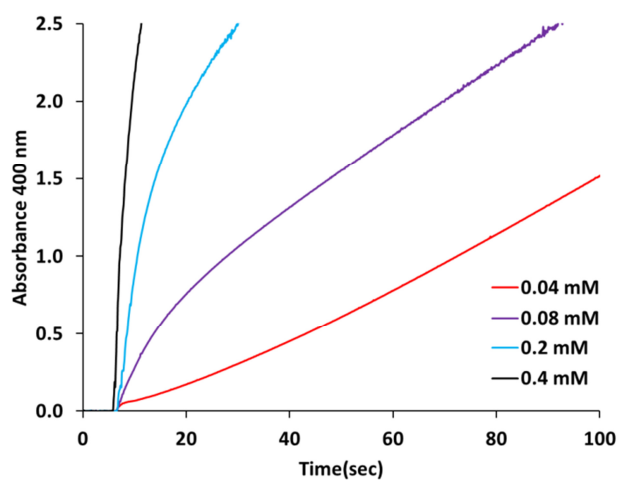


Figure S11. Development in time of the absorption at 400 nm due to 3,5-DTBQ formation, catalyzed by $[\text{Cu}^{\text{II}}_2(\text{L}^1\text{SSL}^1)](\text{BF}_4)_4$ at different copper concentrations: 0.04 mM (red), 0.08 mM (purple), 0.2 mM (blue) and 0.4 mM (black).

S4. Kinetics

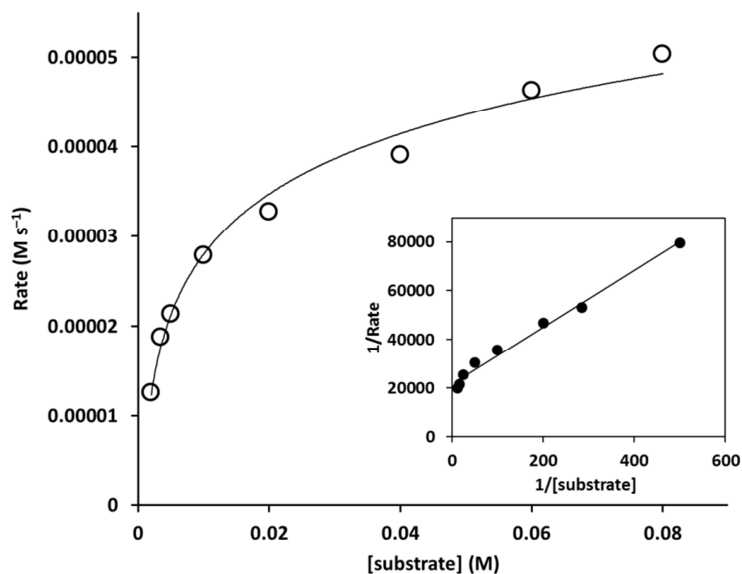


Figure S12. A plot of the substrate concentration vs the catalytic rate for $[\text{Cu}^{\text{II}}(\text{L}^1\text{SCH}_3)](\text{BF}_4)$. The inset shows a Lineweaver-Burk plot for the same complex. Reaction conditions: 0.4 mM [Cu], 20 mM NEt_3 and varying amounts of 3,5-DTBC in 3 mL CH_3CN . $V_{\text{max}} = 0.05 \text{ mM s}^{-1}$; $K_{\text{m}} = 5.3 \text{ mM}$.

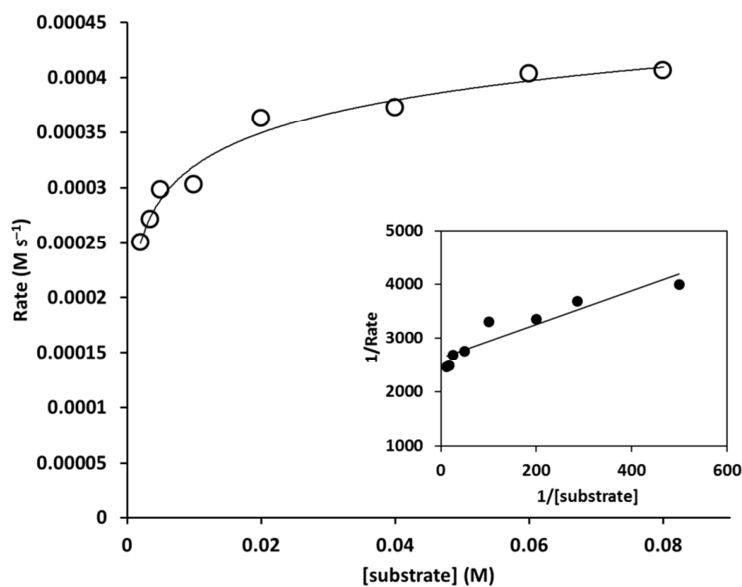


Figure S13. A plot of the substrate concentration vs the catalytic rate for $[\text{Cu}^{\text{II}}_2(\text{L}^1*\text{SSL}^1*)](\text{BF}_4)_4$. The inset shows a Lineweaver-Burk plot for the same complex. Reaction conditions: 0.4 mM [Cu], 20 mM NEt_3 and varying amounts of 3,5-DTBC in 3 mL CH_3CN . $V_{\text{max}} = 0.38 \text{ mM s}^{-1}$; $K_{\text{m}} = 1.2 \text{ mM}$; $k_{\text{cat}} = 6900 \text{ h}^{-1}$.